Journal of Non-Crystalline Solids 482 (2018) 160–169

Contents lists available at ScienceDirect

Journal of Non-Crystalline Solids

journal homepage: www.elsevier.com/locate/jnoncrysol

Linear and nonlinear optical properties of gold nanoparticles doped borate glasses

G. Jagannath[a], B. Eraiah[a,*], K. NagaKrishnakanth[b], S. Venugopal Rao[b]

[a] Department of Physics, Bangalore University, Bangalore 560056, Karnataka, India
[b] Advanced Centre of Research in High Energy Materials (ACRHEM), University of Hyderabad, Hyderabad 500046, Telangana, India

ARTICLE INFO

Keywords:
Gold nanoparticles
Borate glasses
Bandgaps
Z-scan
Nonlinear optical

ABSTRACT

Gold nanoparticles (NPs) embedded in sodium antimony borate glass system were fabricated and their optical, physical, structural, ultrafast nonlinear optical properties were studied and analyzed. Metallic gold NPs were synthesized using thermal reducing agent Sb_2O_3 and demonstrated the reduction mechanism of $Au^{3+}/Au^{+} \rightarrow Au^{0}$ by using reduction potentials of corresponding redox system. UV–Visible spectroscopy measurements have revealed the characteristic surface plasmon resonance (SPR) of Au NPs at ~565 nm, attributed due to interband transition. The micrographs of High-Resolution Transmission Electron Microscopy (HR-TEM) confirmed the existence of uniformly distributed spherical shaped Au NPs with particle sizes in the 8–45 nm range with an average particle size of 25 nm. The ultrafast nonlinear optical properties of gold doped glasses were investigated using the *Z*-scan technique at a non-resonant wavelength (λ = 800 nm, 80 MHz repetition rate) with femtosecond (fs) Ti:sapphire laser pulses. Z-scan measurements of undoped glass depicted are verse saturable absorption (RSA) type of nonlinearity whereas the gold-doped glass demonstrated saturable absorption (SA) kind of nonlinearity due to intraband (sp → sp) transitions. The *Z*-scan data demonstrated that the investigated glasses are potential materials for the applications in nonlinear optics devices, particularly in optical switching devices.

1. Introduction

In recent years, the investigations on nonlinear optical (NLO) materials with ultrafast response, high laser induced damage threshold, large two-photon absorption (2PA) and third order nonlinearities have been attempted since these are crucial for the development of next generation photonic devices. Additionally, materials with good optical switching properties are of great interest for waveguide applications [1]. In particular, glasses containing metal nanoparticles (MNP) have drawn significant importance due to their (i) potential applications in; laser physics [1], optoelectronics [2], photovoltaics [3], nanophotonics [4], wavelength converters, super continuum generators, pulse modulators, high speed-high-capacity optical communication system and high-power-short-pulse broad band fiber laser system [5], (ii) high transparency, high mechanical strength, ease of fabrication in desirable shapes and sizes (iii) the MNP concentration dependent NLO response [1] and (iv) use of glasses as a ultrafast optical switchers and limiters since they have fast response time and high Kerr nonlinearity [6]. Further, noble MNP's have fascinated the materials scientists because of their unique properties, including the high scattering and absorption of light resulted from huge optical field enhancements, high electrical conductivity and excellent catalytic property [7–10]. The resonant oscillation of free electrons of the MNPs in the presence of light also known as surface plasmon resonance (SPR) is the origin for enrichment in optical and NLO properties of MNPs [2]. This SPR usually occurs at visible and infrared (IR) regions resulting in effectual resonant light absorption and scattering within a precise spectral range [11]. These properties can be used to exploit light illumination for a variety of applications including photocatalysis, solar cells, sensors, cancer therapy and biological imaging [12–17]. Particularly, gold (Au) NPs are of significant interest due to their capacity to support SPR phenomena and their unique optical properties and it is also due to its low inherent toxicity, an essential requirement for biological applications [18]. For empowering the optical performance of plasmonic nanostructures, it is necessary to tune the peak position, width, and amplitude since by varying the particle size, shape and the composition the SPR or plasmonic properties of NPs can be controlled [11,15,19]. In the absence of intimate contact with a substrate, the peak position of the plasmonic resonance can be tuned by the nanoparticle size [20], shape [21], composition [22] and refractive index of the surrounding dielectric

* Corresponding author.
E-mail addresses: beraiah@bub.ernet.in (B. Eraiah), soma_venu@uohyd.ac.in (S. Venugopal Rao).

https://doi.org/10.1016/j.jnoncrysol.2017.12.036
Received 6 September 2017; Received in revised form 8 December 2017; Accepted 18 December 2017
Available online 21 December 2017

medium [23].

The NLO properties of the glasses comprising of MNPs fabricated from different routes were generally investigated at the wavelength that corresponds to the wavelength of the SPRs of these particles [1]. Meanwhile, it is practically important to use the optical switches, optical limiters and other components at the wavelengths of the commercially available lasers, such as Nd:YAG (λ = 1064 nm) and Ti:Al_2O_3 (λ = 800 nm). Therefore, it is essential to study their NLO properties not only in the spectral range of their SPRs, but also at the wavelengths of the commercial lasers towards the development of new materials for practical use in integrated optics and laser systems. The importance of these studies has been understood because the materials possessing strong NLO properties in the near IR range are very attractive for the telecommunication applications. Furthermore, compared to continuous wave (CW) and long-pulsed lasers, the femtosecond (fs) lasers have two distinct features: (i) partial elimination of the thermal effects because of high short energy impeachment time and (ii) high localization of laser photons in both time and spatial domains made possible to assist various nonlinear processes. Because of the ultrafast light–matter interaction time and the high peak powers associated with these pulses, the material processing with fs pulses is generally characterized by an absence of heat diffusion [19]. In literature, there are several reports on the NLO properties of MNPs embedded in silica matrix [5], germanate matrix [24], germano-silicate matrix [25,26], boro-silicate matrix [7], heavy metal oxide matrix [27], phosphate matrix [28], sapphire matrix [29], indium tin oxide matrix [30],TiO_2 matrix [31], and $SrTiO_3$ matrix [32]. However, there are few reports on the NLO properties of borate glasses comprising MNPs. Furthermore, borate glasses possess excellent photonic properties such as good transparency, low glass transition temperature (Tg), high density, high thermal expansion coefficient (allowing easy optical fiber fabrication), optimum bandwidth, good infrared transmission, high mechanical stability, high vitrifying ability and is available at low-cost besides unusual capability to dissolve large amounts of other glass formers, modifiers, rare-earths and MNPs or intermediate compounds without reduction of the glass-forming ability [33]. Particularly, borate glasses containing alkali metals are promising for MNPs formation [33]. These borate glasses consist of intermediate-range ordered micro-domains of boroxol group. Such structural disordering in borate glasses leads to an increase in the average B—O distance in both stable oxygen coordinations of boron (i.e. triangular BO_3 and tetrahedral BO_4) [34]. It was recently demonstrated by Youngman et al. [35,36] that near the glass-transition temperature the boroxol rings breakup leads to more open structure in borate glasses. Therefore, alkali borate glasses are an interesting host material for experiments with metallic MNPs formation. The present work reports on optical, structural and ultrafast non-resonant (fs laser operating at wavelength, λ = 800 nm was used) NLO properties of gold doped Sb_2O_3—Na_2O—B_2O_3 glasses.

2. Experimental details

2.1. Samples preparation

The glasses of nominal composition $2Sb_2O_3$–$25Na_2O$–$73B_2O_3$–$xAuCl_3$ (x = 0, 0.005, 0.01, 0.02 mol%, hereafter named as NB–0, NB–1, NB–2, NB–3 respectively) were prepared by melt quench technique. The proper weights of AR grade Sb_2O_3, Na_2CO_3, H_3BO_3, and $AuCl_3{\cdot}HCl{\cdot}xH_2O$ chemicals were mixed homogenously and the composition was taken in a porcelain crucible and kept in high temperature furnace. Initially, the batches were maintained at about 450–500 °C for 30 min for complete decarbonisation of Na_2CO_3 and the decomposition of H_3BO_3 and the temperature was raised and maintained at 1160^0C of about 50 min. The crucibles were shaken frequently at interval of 15 min for a uniform mixing of all the glass constituents. The glass melts were quickly cooled at room temperature by pouring and pressing between two pre-heated brass moulds after the complete melting. The as prepared glasses were ruby in colour and the glasses were polished for further characterization with post annealing of the samples at 350 °C for ~4 h to remove the thermal stresses in glasses. A good reproducibility was achieved in gold doped glasses. The circular disc shaped glass samples with typical thickness of ~1 mm (in particular, the thickness of the NB–0, NB–1, NB–2 and NB–3 glasses were 0.98 mm, 0.95 mm, 0.97 mm and 0.99 mm, respectively) were used for characterization.

2.2. Characterization of the glasses

XRD (Rigaku Ultima IV) measurements using Cu-Kα radiations (λ = 1.54 Å) with copper filters operating at 40 kV and 100 mA, the range of 2θ was 0^0–60^0 with step size of 0.2^0, a resolution of 0.01^0were used to confirm the glassy nature of the samples. The room temperature optical absorption spectra were recorded using PerkinElmer Lambda–35 UV–Vis spectrometer in the range of 200–1100 nm equipped with a deuterium lamp and halogen lamp with a resolution of ± 1 nm. The refractive indices measurements were made using Abbe's refractometer having mono-bromonaphthalene as the contact layer between the sample and prism of the refractometer, and sodium vapour lamp emitting the light of wavelength of 5893 Å (D line) was used as a source of light, the measurements of refractive indices were repeated for consistency and all obtained values were similar with an error of ± 0.0001. Technica G2, F30 High- Resolution Transmission Electron Microscope (HR-TEM) operating at accelerating potential of 300 kV with resolution of 2 Å was used to obtain the structural morphology, size distribution and to verify the existence of gold NPs in the glass matrix. Fourier transform infrared (FTIR) transmission spectra of all glass samples were taken by a Thermo Nicolet, Avatar 370 FTIR spectrometer in the range of 400–4000 cm^{-1} with resolution of 4 cm^{-1} using KBr pellet technique. The ultrafast nonlinear optical measurements were made using *Z*-scan technique [37]. In Z-scan experiments, fs pulses from a Ti:sapphire laser (Chameleon, Coherent Inc., 80 MHz, ~150 fs) were utilized. The wavelength of 800 nm (non-resonant wavelength) was selected in the present experiments. In the far field, a perfect Gaussian profile of the input bean was obtained by spatial filtering. In *Z*-scan measurement, the input beam of 2–mm diameter was focused using 10 cm focal length convex lens and the glass sample was placed on a 10-μm resolution translation stage. The data was collected manually using a detector (Thermal Sensor-Field Max, Coherent). Since the Z-scan technique is a sensitive technique, to avoid the errors in the collected data, the samples having high polish, uniform thickness were used for measurements and the measurements were repeated with the same intensity. The obtained NLO coefficients were within the experimental estimated error of ± 10% for both open aperture and closed aperture data. The main sources of errors in such measurements are from the peak intensity estimation, laser pulse to pulse fluctuations, and fitting errors.

3. Results and discussion

3.1. X-ray diffraction and UV–Vis absorption spectroscopy

The absence of sharp crystallization peak and presence of a broad hump at 40^0–55^0 confirms the glassy nature of the samples. Fig. 1 presents the typical XRD patterns of all the samples and are nearly same. The concentration of gold in present glasses is very low and, therefore, no characteristic peak of Au was evident in the spectra [38]. The absorption spectra of glasses containing MNPs are always very much responsive to the size, shape and interparticle distance and dielectric function of the MNPs [38,39]. The optical absorption spectra for glasses doped with different concentration of gold displayed in Fig. 2 (a), in which inset showing the absorption spectrum of undoped (NB–0) glass. The undoped glass did not demonstrate any absorption band. However, the clear proof of SPR absorption band near 565–597 nm (due to the interband transition from the 'd' band to the

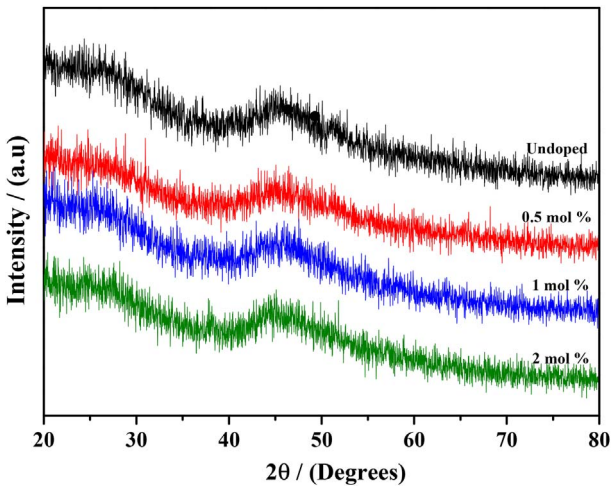

Fig. 1. XRD patterns of undoped and doped glasses.

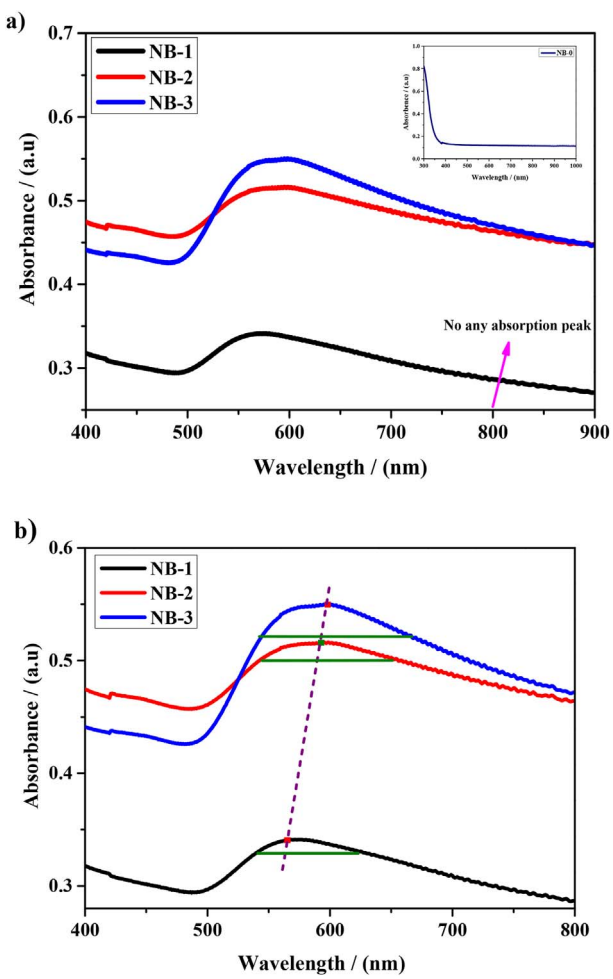

Fig. 2. (a) Optical absorption spectra of NB glass doped with different concentration of gold, inset representing the absorption spectrum of undoped glass.
(b) Position and broadening of SPR peak at different concentration of gold, dashed line representing weak red shift in SPR peak and horizontal solid line representing broadening of SPR peak with increase in gold content. (For interpretation of the references to colour in this figure legend, the reader is referred to the web version of this article.)

Fermi level [40]) is observed for samples doped with Au, which discloses the existence of nano-sized Au particles.

The optical absorption coefficients α (λ) of the samples were obtained by using the equation given below [41]:

$$\alpha(\lambda) = 2.303\left(\frac{A}{d}\right) \tag{1}$$

where, 'A' and 'd' are the absorbance and the thickness of the glass samples, respectively.

The measurement of absorption edge is important, especially in connection with the theory of the electronic structure of amorphous materials. The higher energy parts of the spectra, particularly those associated with the integrand electronic transition will provide information about the electronic states. In this respect, the electrons are excited from a filled band to an empty one by photon absorption and as a consequence a marked increase in the absorption coefficient 'α' will result [42]. The onset of this rapid change in 'α' is called fundamental absorption edge and the corresponding energy is defined as the energy gap. The relation between 'α' and the photon energy of the incident radiation 'hν' was interpreted by Davis and Mott [43] and can be written in general form as:

$$\alpha h\nu = B(h\nu - E_{opt})^n \tag{2}$$

where, 'α' is the absorption coefficient, 'hν' is the incident photon energy, B is constant called band tailing parameter, E_{opt} is the energy of the optical band gap, 'n' depends on the type of transition (direct or indirect) taking the values $n = 2$, 3, 1/2, and 1/3 which correspond to indirect allowed, indirect forbidden, direct allowed, and direct forbidden transitions respectively, n also depends on the nature of the material (crystal or amorphous). For amorphous materials, indirect transitions are valid according to Tauc relation, i.e. the power part $n = 2$, because one important difference between amorphous and crystalline solids is that, there is a sharp well-defined lattice absorption edge E_{opt} for crystalline solids whereas in amorphous materials, the absorption edge has a finite slope. Thus, when analyzing the variation in optical absorption with respect to the photon energy, $n = 2$ is valid [44]. To estimate the values of direct (E_g^{dir}) and indirect (E_g^{indir}) bandgap energies, the linear regions of $(\alpha h\nu)^2$ v/s hν and $(\alpha h\nu)^{1/2}$ v/s hν are extrapolated to meet hν at $(\alpha h\nu)^2 = 0$ and $(\alpha h\nu)^{1/2} = 0$ as shown in Fig. 3(a) and (b) respectively.

It is well known that, the SPR peak of MNPs depends on the refractive index of the surrounding media, concentration of metallic NPs as well as the size and shape of the MNPs inside the glass matrix. From the data presented in Fig. 2(b) it is evident that the SPR peak of Au NPs is shifted to longer wavelengths [from 565 to 597 nm i.e., a weak red shift in SPR peak of Au NPs, represented by dashed line in Fig. 2 (b)] with increase in gold content from 0.005 mol% to 0.02 mol% manifesting the formation of larger Au NPs by Ostwald's ripening process [45]. The refractive index is increases (refer Table 1) with increase in gold concentration, this increase in refractive index is attributed to the fact that the increase in the mol% of gold results in increase in density of Au NPs and also growth of Au NPs. Thus it was concluded that the SPR peak of Au NPs is red-shifted with enhancement in refractive index of the glasses and this observed red-shift of the SPR peak of Au NP with the increase of the refractive index is related to resonance condition, which is satisfied at higher values of the wavelength of the incident light due to the increase of the wave vector of the surface plasmon mode [25,46,47]. Similar observations (i.e. red-shift of plasmon band of MNPs with increase in refractive index of glass matrices) were made by Ju et al. [46,48], Amjad et al. [49], Ghoshal et al. [38] and many others in the glass matrices comprising MNPs. In addition to the red-shift, the broadening of these SPR peaks of gold NPs [represented by horizontal solid lines in Fig. 3(b)]are attributed to the increase in Au NPs density and decrease in Au–Au interparticle distance ($d_{Au\text{-}Au}$) i.e., Au NPs spacing decreases with increase in mol% of the Au (refer Table 1) [24,50]. According to Maxwell–Garnett theory (MG theory), the SPR peak is shifted through electromagnetic coupling, therefore, both the coupling between the surface plasmons of closely spaced Au NPs and aggregation of Au NPs (which led to larger spherical particles) were responsible for observed red shift and broadening of the SPR peak of Au NPs in studied

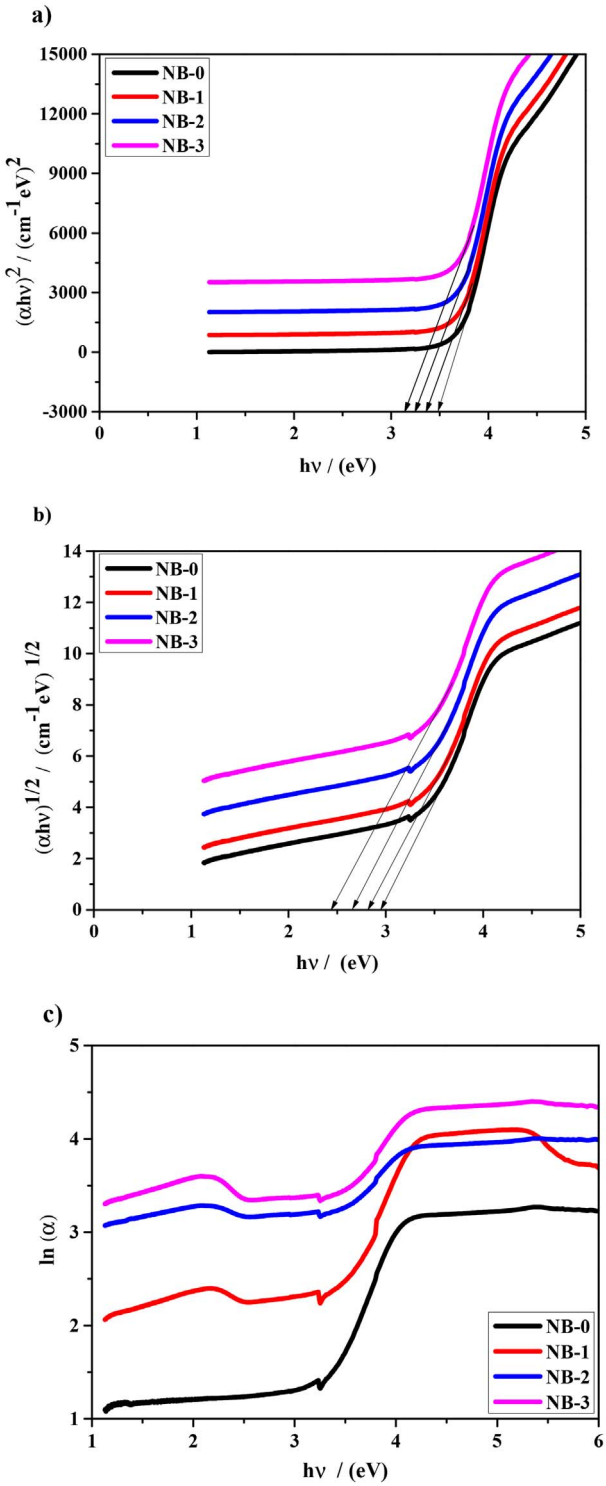

Fig. 3. (a) Plot of $(\alpha h\nu)^2$ v/s $h\nu$ for direct bandgap energy measurements. (b) Plot of $(\alpha h\nu)^{1/2}$ v/s $h\nu$ for indirect bandgap energy measurements. (c) $h\nu$ dependence on ln(α) for Urbach energy calculations.

glasses [51].

The increase is in refractive index also responsible for reductions of the optical band gaps as shown in Fig. 3 (a) and (b) [38]. It is explained that, the electronic and spectral features of the MNPs yield basic changes as compared to that of bulk materials when the diameters of the MNPs reduced to 2–20 nm [38] and this kind of behaviour arises from the quantum size effects, can affect the electronic band structures and therefore, alters the effective band gap [52].

3.2. Physical properties

Density of the samples were measured using the Archimede's principle with toluene as the immersing liquid and was calculated using the expression,

$$\rho = \frac{W_a}{W_a - W_b} \times \rho_l \tag{3}$$

where, 'W_a' and 'W_b' are the weights of the sample in air and that of in toluene immersion ($\rho_l = 0.8669\ g\ cm^{-3}$) respectively. The best chemical stability against hygroscopic attack of the glasses and somewhat low toxicity of toluene made to prefer it as immersion liquid [38], the density measurements were repeated for consistency by calibrating the instrument (weighing balance) at each and every time, and all yielded values are almost same at an error of ± 0.004.

The molar volume (Vm) of the glasses was calculated from the expression [53],

$$V_m = \frac{M_i}{\rho} \tag{4}$$

where, 'M_i' and 'ρ' are the average molecular weight and the density of the glasses respectively.

The molar refractivity (R_M) was obtained from the expression [54],

$$R_M = \frac{\epsilon - 1}{\epsilon + 2}[V_m] \tag{5}$$

where, 'V_m' and 'ϵ' are the molar volume and the dielectric constant of the samples respectively.

The electronic polarizabilities (α_e) of the glasses was calculated with the help of Lorentz–Lorenz equation [54],

$$\alpha_e = \frac{3}{4\pi N_A}(R_M) \tag{6}$$

where, 'N_A' is the Avogadro's number.

The atomic concentration of Au was calculated using,

$$N = \frac{x \times \rho \times N_A}{M_i} \tag{7}$$

where, 'x' is the mol% gold.

Polaron radius of gold atoms was calculated from the expression,

$$r_p(\text{Å}) = \frac{1}{2}\left(\frac{\pi}{6N}\right)^{\frac{1}{3}} \tag{8}$$

Inter particle distance of gold NPs ($d_{Au\text{-}Au}$) was calculated from the equation,

$$d_{Au-Au}(\text{Å}) = \left(\frac{1}{N}\right)^{\frac{1}{3}} \tag{9}$$

Dielectric constant of the glasses was calculated using the relation,

$$\epsilon = n^2 \tag{10}$$

where, 'n' is the refractive index of the glass samples.

Linear optical susceptibility was estimated using,

$$\chi^{(1)} = \frac{n^2 - 1}{4\pi} \tag{11}$$

The complete idea about the physical properties is necessary to analyze the changes in the structure of the glass system. Fig. 3(a) and 3(b) depicts the $h\nu$ dependency on $(\alpha h\nu)^2$ and on $(\alpha h\nu)^{1/2}$ for direct and indirect band gap energies respectively for base and Au doped NB glasses. The Urbach energy was calculated from the inverse of the slope of ln (α) v/s $h\nu$ and Fig. 3(c) represents the plot of ln (α) v/s $h\nu$ for undoped and Au doped glasses. The noticeable decrement in direct optical band gap energy (E_g^{dir}) from 3.469 to 3.131 eV and indirect optical band gap energy (E_g^{indir}) from 2.937 to 2.428 eV (shown in Table 1) with the increase of Au NPs concentration is due to an increase

Table 1
Physical, optical and inter-nuclear property of NB glasses at different concentration of gold.

Properties (± error limits)	NB-0	NB-1	NB-2	NB-3
Physical properties				
Average molecular weight, M ($gmol^{-1}$)	72.152	72.167	72.184	72.217
Density, ρ (gcm^{-3}) (± 0.002)	2.466	2.497	2.468	2.415
Molar volume, V_m ($cm^3 mol^{-1}$) (± 0.001)	29.258	28.901	29.247	29.903
Refractive index, n (± 0.001)	1.620	1.625	1.631	1.637
Dielectric constant, ϵ(± 0.001)	2.624	2.640	2.660	2.679
Molar refractivity, R_M (cm^{-3}) (± 0.002)	10.278	10.218	10.419	10.734
Electronic polarizability, α_e($\times 10^{-24}$ cm^3) (± 0.001)	4.073	4.0495	4.129	4.254
Linear susceptibility, $\chi^{(1)}$ (± 0.001)	0.129	0.131	0.132	0.134
Optical properties				
Direct optical band gap, E_g^{dir} (eV) (± 0.002)	3.469	3.346	3.245	3.131
Indirect band gap, E_g^{indir} (eV) (± 0.002)	2.937	2.80	2.639	2.428
Urbach energy, E_U (± 0.001)	0.413	0.475	0.823	0.840
Position of SPR peak of gold (nm)	–	565	590	597
Inter-nuclear properties				
Concentration of gold (mol %)	0	0.005	0.01	0.02
Au atoms concentration, N ($\times 10^{20}$ atoms/cm^3) (± 0.0001)	–	1.0421	2.0592	4.0281
Au-Au interparticle spacing, $d_{Au\text{-}Au}$ (nm) (± 0.0001)	–	2.1581	1.7202	1.3761

in the disorder and decrease in the rigidity in the NB-glasses [55]. However, the Urbach energy (E_U) increases from 0.413 to 0.840 eV as the Au NPs concentration increases from 0.005 to 0.02 mol% manifests the degree of disorder present in the glass samples [56]. As increase in the concentration of gold, the refractive index is increases from 1.620 to 1.637 and is imputed to the notable changes in the structure of the glass, which in turn signifies the higher polarizability [57]. From the literature it is found that, the vibrations of boron and oxygen atoms in glass structure affected by the addition of NPs in to the glass matrix which introduces large scale disruptions in the glass network by the conversion of bridging oxygens to non-bridging oxygen [58], these created non-bridging oxygens in turn responsible for increase in refractive indices by contributing higher polarizability over the covalent bonds of bridging oxygens [56].

The effect of Au NPs on the density and molar volume of NB glass systems is shown in Fig. 4. The decrease in glass density from 2.466 to 2.415 g cm^{-3} and increase in molar volume from 29.258 to 29.903 $cm^3 mol^{-1}$ with increase in mol% of Au NPs is ascribed to the contraction in structural network of the glasses and is due to the participation of Au NPs in the free space region of the network structure and the elongation in the bond length or an increase in the interparticle spacing respectively [38]. The increment in molar refractivity from 10.278 cm^{-3} to 10.734 cm^{-3} is proportional to the polarizability of the glass samples [59].

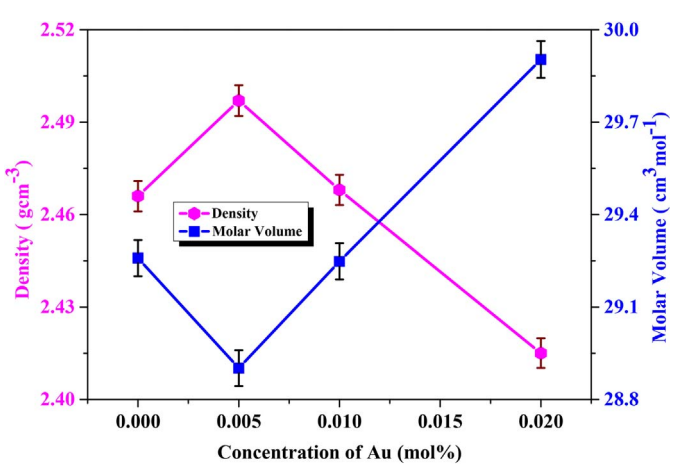

Fig. 4. Variation of density and molar volume with varied concentration of gold. (For interpretation of the references to colour in this figure legend, the reader is referred to the web version of this article.)

3.3. Fourier transform infrared (FTIR) spectroscopy and high resolution transmission electron microscopy (HR-TEM) analysis

The addition of alkali and/or other metal ions into a well-known glass former B_2O_3 results in the formation of several BO_3^{3-} groups and it brings about the changes in the boron co-ordination from three-to four-membered one, which generates several BO_3 units such as diborate, triborate and tetraborate. Subsequently, the addition of gold NPs modifies the bonding between ligands [38]. The FTIR spectra of all the glass samples have been recorded for identifying the network structure of the glasses and are shown in Fig. 5. The FTIR spectra's of different concentration gold shown in Fig. 5 are nearly same, means that, Au NPs do not change the structure of present glasses and also four to five absorption peaks with the peaks are sharp, medium and broad can be observed in Fig. 5. The combined effect of vibrational states of high degeneracy, lattice dispersion thermal broadening and mechanical scattering from the powder samples gives rise broad bands in oxide spectra [60]. The 806 cm^{-1} frequency is a characteristic frequency of boroxol ring in pure B_2O_3 glasses [60], the absence of absorption peak at 806 cm^{-1} in FTIR spectra of present glasses indicates the absence of boroxol ring formation, because the Krogh Moe's model [61] proposed that, the structure of borate glass consists of a random network of

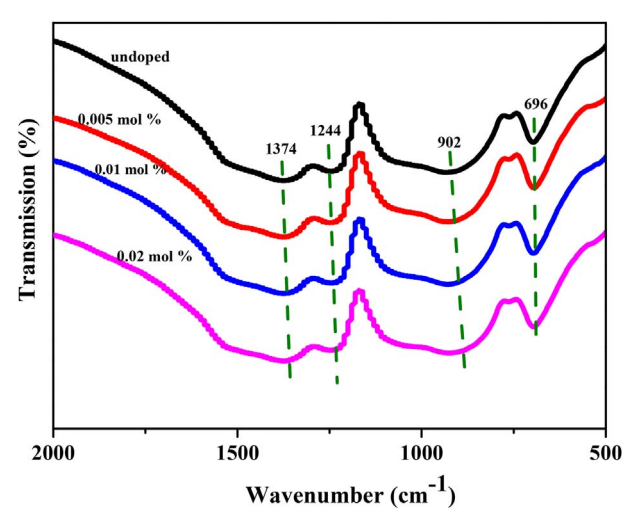

Fig. 5. FTIR spectra of NB glasses at different concentration of gold. (For interpretation of the references to colour in this figure legend, the reader is referred to the web version of this article.)

planar BO_3 triangles with a certain fraction of six membered (boroxol) rings. It concludes that, the present glass system consists of only BO_3 and BO_4 groups. The same kind of behaviour is also observed in B_2O_3–Li_2O glasses [62,63]. These groups may be attached in the form of random network, resembles to the continuous substitution of boroxol ring by BO_3 and BO_4 groups [60].

The vibrational modes in borate glass structure is predominantly active in three IR regions, which are: (i) the bands at 1200–1600 cm^{-1}attributed to the asymmetric stretching relaxation of the B—O band of trigonal BO_3 units (ii) the bands lies between 800 and 1200 cm^{-1} and are ascribed to the starching of B—O bonds in tetrahedral BO_4 units and (iii) the bands around 700 $cm^{-1}$are attributed to B—O—B linkages bending in the borate networks [64]. The band at around 1374 cm^{-1} is assigned to stretching vibrations of B—O bonds of various trigonal $(BO_3)^{3-}$ units [60]. The shoulder at around 1244 cm^{-1} may arise from stretching vibrations of B—O bonds of $(BO3)^{3-}$ unit in metaborate and orthoborates chains. It is reported that, in IR spectra of Na_2O—B_2O_3—SiO_2 and Na_2O—B_2O_3—PbO glasses, the band at around 995 cm^{-1} and 993 cm^{-1} is ascribed to a stretching vibration of B—O—Si and B—O—Pb linkage respectively [60,65]. Similarly, the presence of broad absorption band at 902 cm^{-1}inthe present case may be assigned to a stretching vibration of B—O—M (B—O—Sb) linkage; M represents a metal ion i.e. Sb. The absorption band at 696 cm^{-1} is assumed to be due to the combination of bending vibrations of B—O—B linkages in BO_4 and symmetric stretching Sb—O—Sb vibrations of SbO_3 trigonal pyramids with Cs or C_2 symmetry (Table 2) [60,65].

The particle sizes of Au NPs were investigated using the HR-TEM. The micrographs of HR-TEM of NB-2 glass (doped with 0.01 mol% of Au) are shown in Fig. 6(a) and (b). The size distribution and morphology of Au NPs have been analyzed using imageJ software. Fig. 6(a) illustrates the uniformly distributed Au NPs and Fig. 6(b) depicts that the Au NPs are spherical in shape in NB glasses. Histogram for size distribution of Au NPs in NB glasses is shown in Fig. 6(c). Many spherical shaped Au^0 NPs dispersed homogeneously in the glass matrix with wide size distribution ranging from 8 nm–45 nm with an estimated average particle size of 25 nm have been observed from HR-TEM micrographs. The spherical rings around the central bright region present in SAED pattern shown in Fig. 6(d) also confirms the existence of Au^0 nanocrystallites in the glass matrix. Crystalline Au NPs with fringe spacing of 0.20 nm shown in Fig. 6(e) corresponds to the (2 0 0) plane of the face centred cubic (FCC) structure of gold (JCPDS card no. 4–784) which again discloses the generation of Au^0 crystallites in the Au-glass nanocomposites. Here it may be noted that, these Au^0nanocrystallites are not detectable by XRD analysis since the concentration of gold is very small.

With the help of reduction potentials (E^0) of the respective redox systems present in the glass system, the probable mechanism of reduction of Au^{3+} to Au^0 by Sb^{3+} can be explained [66,67]. The reduction potentials of the multivalent elements in glasses are highly dependent with temperature. Because of unavailability of the values of reduction potential for antimony and gold at high temperatures, the room temperature E^0values for simple systems at equilibrium with air are used here to explain the reduction mechanism [66,67].

$$Sb^{5+}/Sb^{3+},\ E^0 = 0.649\ V \tag{12}$$

$$Au^{3+}/Au^0,\ E^0 = 1.498\ V \tag{13}$$

Here, the reaction $3Sb^{3+} + 2Au^{3+} \rightarrow 3Sb^{5+} + 2Au^0$ ($E^0 = 1.05$ V and free energy (ΔG) around -608 kJ) is the only conceivable spontaneous reduction reaction [66]. Hence, the negative free energy of reduction reaction saying that, this reaction is spontaneous and thermodynamically feasible i.e. Sb^{3+} reduces Au^{3+} to Au^0 and it itself is oxidized to Sb^{5+}. With this the reduction of Au^{3+} to Au^0 is confirmed with the help of reduction potentials.

Further, Ju et al. [5] have been reported that the presence of reducing agent in the glassy matrix effectively converts Au ions to Au MNPs by providing reduction condition in the glass matrix during the fabrication. However, there is an abundance of OH (even at high temperature) and O_2 in the glass matrix and, therefore, there are chances of $[Au(OH)_4]^-$ or $NaAuO_2$ formation in the glasses. The results of Smithies et al. [68] have proved that the sodium also acts as an alternative reducing agent, which forms stable Au MNPs of smaller size, in the present glasses concentration of sodium 25 mol% (quite high). Hence, it can be thought that sodium also plays a role in the conversion of $[Au(OH)_4]^-$ or $NaAuO_2$ to Au NPs. Furthermore, Lusvardi et al. [69] demonstrated that (for the case of $15CaO$–$5P_2O_5$–$80SiO_2$–xAu_2O, where x = 1 mol% of Au_2O), Au particles in the Au-containing glass samples play an hydrophilic role. Nonetheless, to confirm the formation of 100% Au NPs in these glasses further detailed studies will be necessary to identify the exact mechanisms responsible for such processes.

Table 2
IR band assignments for respective glass samples.

Glass samples and wave numbers in cm^{-1}				Band assignments
NB-0	NB-1	NB-2	NB-3	
1374	1369	1369	1365	B—O stretching vibrations of various trigonal $(BO3)^{3-}$ units
1244	1244	1240	1238	B—O stretching vibrations of $(BO3)^{3-}$ units in metaborate and orthoborates chains
902	902	902	902	Stretching vibration of B—O—Sb linkage,
696	692	692	691	Bending vibrations of B—O—B linkages in BO_4 and symmetric stretching Sb—O—Sb vibrations of SbO_3 trigonal pyramids.

3.4. NLO properties

The strong NLO properties and the ultrafast response times associated to the SPR of metal nanoparticles in glasses makes them potential materials for the applications in photonic devise [70]. However, studying the NLO properties at non-resonant wavelengths is important towards device applications. Hence, the NLO properties of present glasses have been studied using *Z*-scan technique with fs Ti:sapphire laser operating at the wavelength 800 nm (non-resonant wavelength, since there is no any absorption peak in this region). The Z-scan measurements of open aperture (OA) and closed aperture (CA) type were performed to obtain the nonlinear absorption and nonlinear refraction coefficients respectively.

The nonlinear absorption parameters can be obtained by fitting the experimental OA *Z*-scan data with the multi-photon absorption (MPA) equation given by Sutherland et al. [37,71,72],

$$T_{OA}(nPA) = \frac{1}{[1 + (n-1)\alpha_n L_{eff}(I_{00}/(1 + (Z/Z_0)^2))^{n-1}]^{1/n-1}} \tag{14}$$

where, α_n is the effective MPA coefficient ($n = 2$ for 2PA; $n = 3$ for 3PA, and etc.) and I_{00} is the intensity of the input irradiance. The theoretical equation merely for two-photon absorbers yielded when retained only 2PA term in above equation

$$T_{OA}(2PA) = \frac{1}{1 + \alpha_2 L_{eff}(I_{00}/(1 + (Z/Z_0)^2))} \tag{15}$$

where, the effective path length (L_{eff}) in the sample of length L for 2PA is $L_{eff} = \frac{1-e^{\alpha_0 L}}{\alpha_0}$, I_{00} is the peak intensity in the input beam, Z is the sample position, $Z_0 = \pi\omega_0^2/\lambda$ is the RayleighRange, ω_0 is the beam waist at the focal point (Z = 0), λ is the wavelength of the laser light used for the experiment.

The closed aperture *Z*-scan data was fitted the with following equation [72],

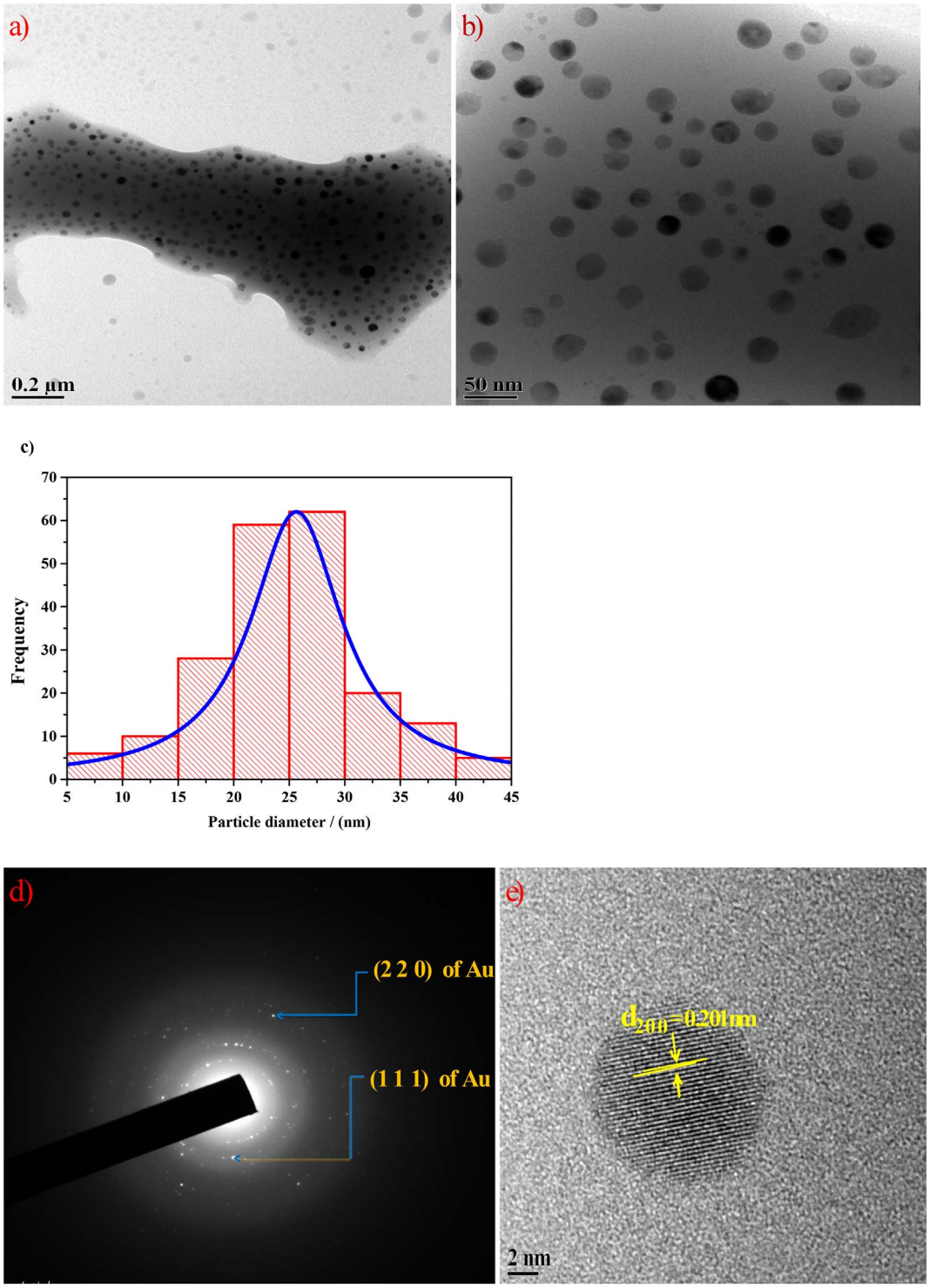

Fig. 6. (a) and (b) HR-TEM images of NB glasses doped with 0.01 mol% of gold. (c) The histogram of Au NPs. (d) SAED pattern Au NPs. (e) Planes of Au NPs and fringe spacing between them. (For interpretation of the references to colour in this figure legend, the reader is referred to the web version of this article.)

$$T_{CA} = 1 + \frac{4\Delta\Phi_0(Z/Z_0)}{[1 + (Z/Z_0)^2][9 + (Z/Z_0)^2]} \quad (16)$$

where, $\Delta\Phi_0$ is the phase difference of the laser beam caused due to nonlinear refraction and is obtained by fitting the CA Z-scan experimental data with above equation. The nonlinear refractive index obtained using,

$$n_2(m^2W^{-1}) = \frac{|\Delta\Phi_0|\ \lambda}{2\pi I_{00} L_{eff}} \quad (17)$$

Fig. 7(a) and (b) illustrate the open and closed aperture Z-scan signatures for undoped glasses [in Fig. 7(a) and (b), the open circles represents the experimental data while the solid lines are theoretical fits]. In Fig. 7(a), OA Z-scan data of undoped glasses is established a valley in the transmittance as the sample reached the focal point (Z = 0) and that valley represents pure RSA. The 2PA coefficient (α_2) was evaluated by fitting the experimental OA Z-scan data with Eq. (15) and the evaluated value of α_2 is $13.5 \times 10^{-12}\ mW^{-1}$. The pre-focal dip and the post-focal peak shown in Fig. 7(b) is the signature of CA Z-

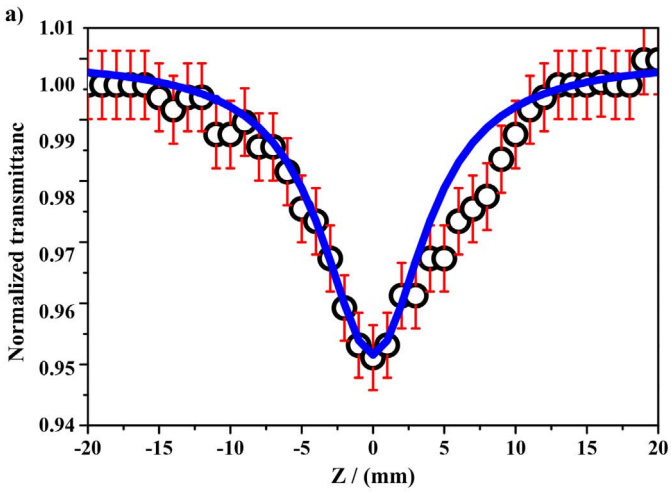

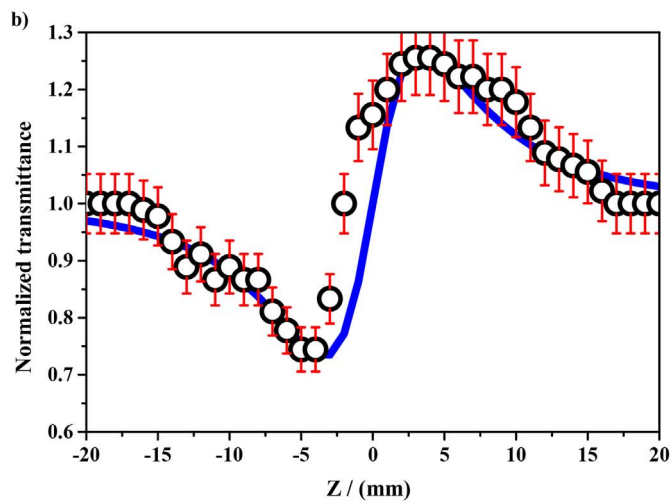

Fig. 7. *Z*-scan signatures of undoped NB glasses (a) Open aperture Z-scan curve (b) Closed aperture Z-scan curve. The open circles represent the experimental data while the solid lines are theoretical fits.

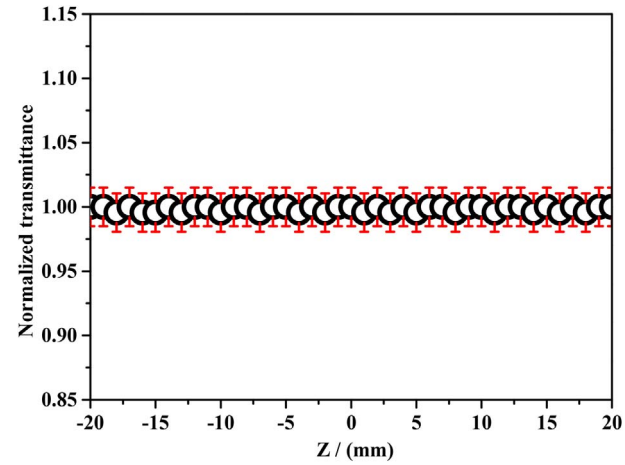

Fig. 8. Open aperture Z-scan data for $25Na_2O$-$75B_2O_3$ glass.

scan data for undoped glasses and is indication of positive nonlinear refraction, which is attributed to self-focusing nonlinearity. The CA Z-scan experimental data was fitted with Eq. (16) to calculate the nonlinear refractive index (n_2) and estimated value of n_2 is $1.189 \times 10^{-17} m^2 W^{-1}$. Generally, the division of NLO phenomena can be done as the resonant and non-resonant nonlinear effects based on the real or virtual states are involved in photo excitation. Both the effects can contribute to the optical nonlinearity in inorganic glasses. The NLO property of positive type is due to the hyperpolarizabilities of the constituents present in the glass composition like the heavy metal cations (such as Pb^{2+}, Bi^{3+}, Sb^{3+},W^{5+},Te^{4+}, Ge^{4+},Nb^{5+}, Si^{3+} etc.) transition-metal ions, bridging and non-bridging oxygens [73]. Xinhua Zhu et al. [73] further demonstrated that, the glasses containing heavy metal oxides (HMO) results in small 2PA and high nonlinear refractive index due unusual hyperpolarizability of non-bridging lone pair electrons of heavy metal ion and effective screening of outer electron from the nucleus under the impact of applied optical electric field. Thus, the observed small 2PA and high nonlinear refractive index (comparably) of undoped glasses is ascribed to the large hyperpolarizability of the non-bonding lone electron pairs of Sb^{3+} and the many filled inner electronic shells of Sb^{3+} ion screen the outer electrons efficiently from the nucleus, thus promoting large charge displacements to occur due to the domination of an applied optical field. The anharmonic effects originate from such large displacements are manifested by the high nonlinear refractive index (n_2) of glasses containing antimony. Also, from the structural (FTIR) analysis discussed in earlier section, the present glass system have Sb—O—Sb and B—O—Sb local structures, these local structures are also responsible for observed nonlinearity in undoped glass [64]. We also measured the NLO properties of $25Na_2O$–$75B_2O_3$ in OA *Z*-scan under same laser exposure, in which no change in the transmitted intensity as the sample moved along the Z-direction has been observed and is shown in Fig. 8. Therefore, the observed nonlinearity in undoped glasses is only due to the presence of Sb^{3+}. The same kind of nonlinearity has also been observed by Rajaramakrishna et al. [74] for undoped and untreated lanthanum lead borate glasses under 532 nm, nanosecond (ns) laser excitation and by Almedia et al. [27] for undoped HMO (GeO_2–Bi_2O_3) glasses under 500 nm, fs regime.

The open and closed aperture Z-scan results of the NB-1 glasses are depicted in Fig. 9 (a) and (b) respectively [in Fig. 9(a) and (b), the open circles represent the experimental data and solid lines represent the theoretical fits]. The typical peak symmetric about the focal point showed by OA Z-scan profile is the sign of saturable absorption and it reveals the nonlinear absorption of negative type. A same type of saturable absorption nonlinearity was observed by Rajaramakrishna et al. [74] in the case of lanthanum lead borate glasses doped with gold NPs after the heat treatment at 550 °C at different durations and by Almedia et al. [27] for HMO glasses doped with Au after annealing at 420 °C of about 3 h. The values of 2PA coefficient (α_2) of undoped glasses and saturation intensity of gold doped glasses is found to be comparable with those reported in literature for glasses [74,27]. The values of refractive indices of present glasses are again comparable with those in reported in references [27,75].

In noble MNPs, the NLO properties originally arise from intraband and interband transitions. The transition between the levels in the d-band which are just below the Fermi level and the conduction band results in the interband transition. The transition arises from ground state to the excited state in the conduction band yields the intraband transition. Initially the electrons are stimulated from ground state to the excited state at which they then become free carriers (SPR absorption), this process is subsequently followed by the broad band absorption of these free carriers (free carrier absorption, FCA), finally through electron-phonon interaction, electron-electron coupling and phonon–-phonon relaxation the stimulated electrons decay to the ground state [76]. The intensity is very weak when the glass sample is far from the focal point and this weak intensity unable to cause any nonlinearity, thus the transmitted intensity is unity. The intensity is increases when glass sample is moved towards the focal point and this mild intensity can able to induce the plasmon oscillation of the electrons within the conduction band. Hence the greater number of the nanoparticles is

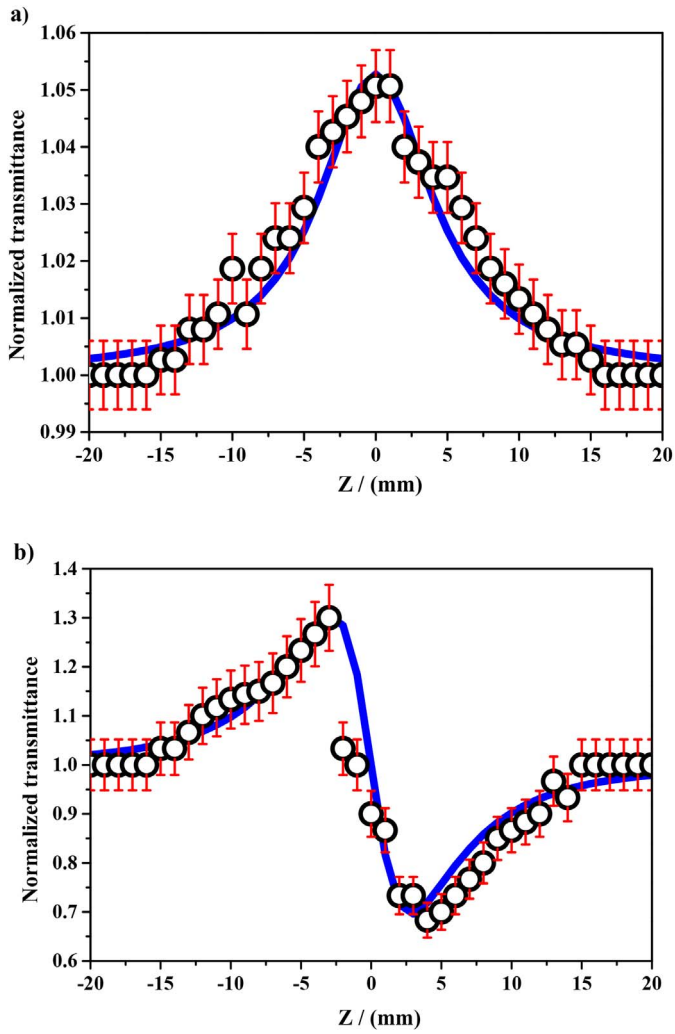

Fig. 9. Z-scan signatures of NB-1 glasses (doped with 0.005 mol% Au) (a) OA Z-scan curve (b) CA Z-scan curve. The open circles represent the experimental data and solid lines representing the theoretical fits.

geared up to the excited state results in smaller population of the ground state, which bleaches the ground state plasmon absorption band. Therefore, the transmittance will be a maximum at this intensity level, result in SA (hump) kind of behaviour [77]. For gold NPs, the first excited transition usually occurs at 6700 Å (1.52 eV) due to intraband (sp → sp) transition. The peak at 4500 Å (2.63 eV) attribute to intraband (sp → sp) and interband (d → sp) mixed transitions, and that at 4000 Å (2.91 eV) is essentially from an interband transition (d → sp) [78]. The excitation of free valence electrons near the Fermi surface known as intraband transition and is energetically admissible even with photons of low-energy, whereas the transition of the electrons arises from the d-band to the conduction band is interband transition, which require photon of higher energy [77,78]. However, in our *Z*-scan experiment, the laser wavelength of excitation is 800 nm (1.55 eV) which is obviously smaller than 2.91 eV and near to 1.85 eV and further the peak intensity of the laser pulse maintained while during the experiment was of about 5.2×10^8 Wcm^{-2}. Thus, the intraband (sp → sp) transition is dominant in gold doped glasses and which depletes the electrons near the Fermi surface causing SA nonlinearity.

From Table 3, it is evident that the value of negative nonlinear refractive index (n_2) gold doped glasses increases as the concentration of gold increases. This may be attributed to the fact that the number gold NPs increases when the concentration of gold increases, representing that more number of Au NPs are contributing to the enhancement of nonlinear refractive index. The enhancement in the nonlinear refractive index at 800 nm (fs) with the increase of $AuCl_3$ concentration in sodium antimony borate glasses also attributed to the increase of the NBOs in glasses as amount of gold increases. However, with fs MHz excitation there are some thermal effects expected hence the studies with kHz excitation will be taken up in near future. From the application point view, the glasses having high nonlinear refractive index and small 2PA coefficient can be considered as a promising material for ultrafast optical switch in an optical fiber communications system. Since the present glasses exhibited relatively low 2PA, hence the present glasses are suitable for optical switching devices or optical switches.

4. Conclusions

Au NPs have been successfully fabricated with conventional melt quench method in sodium antimony borate glasses. We systematically investigated the optical, physical, structural and ultrafast nonlinear optical properties of the NB glasses doped with different concentration of gold. The glassy nature of the glass samples has been verified by XRD patterns. The optical absorption spectra of glasses doped with Au NPs exhibit SPR plasmon band at around 565–597 nm due to the interband transition and a weak red shift in gold plasmon band have been observed with increase of gold content, which is attributed formation of larger Au NPs by Ostwald's ripening process with increase of Au concentration. The noticeable decrease in optical band gap energy and increase in Urbach energy with respect to gold concentration attributed to an increase in the disorder and decrease in the rigidity. From HR-TEM it was clear that, Au NP in FCC crystal system have uniformly dispersed in the glass matrix and the size distribution of these NPs ranged from 8 to 45 nm with the average particle size about 25 nm. However, the gold crystal peak in XRD has been not observed due to low concentration of gold. The broad absorption bands at 902 and 696 cm^{-1} in FTIR spectra and *Z*-scan results of undoped glass reveals that, the Sb^{3+} is effectively entering in to the glass network though its concentration is very less. The NLO properties of the glasses were determined using Z-scan method at the wavelength of 800 nm using fs pulses. The undoped glass exhibited positive nonlinearity and is ascribed to Sb—O—Sb and B—O—Sb local structures, whereas the glasses doped with gold presents negative nonlinearity. The nonlinear absorption observed in gold doped glasses attributed to the intraband (sp → sp) transition. The enhancement in the negative nonlinear refractive index with increase of gold concentration is due to increase of the NBOs in glasses as content of gold increases. The ultrafast Z-scan studies of the present glass system revealed that, the studied glasses are suitable for optical switching devices like passive mode locking, optical

Table 3
Summary of NLO coefficients obtained from Z–scan results of NB glasses. n_2, α_2, and I_S represents nonlinear refractive index, 2PA coefficient and saturation intensity, respectively.

Samples	n_2 ($m^2 W^{-1}$)	α_2 (mW^{-1})	I_S (Wm^{-2})
NB-0	$1.32 \pm 0.13 \times 10^{-17}$	$13.5 \pm 0.14 \times 10^{-12}$	–
NB-1	$-2.7 \pm 0.27 \times 10^{-16}$	–	$7.42 \pm 0.74 \times 10^{10}$
NB-2	$-3.1 \pm 0.31 \times 10^{-16}$	–	$6.71 \pm 0.67 \times 10^{10}$
NB-3	$-3.8 \pm 0.38 \times 10^{-16}$	–	$4.23 \pm 0.42 \times 10^{10}$

Q-switching of lasers i.e. in the generation short pulses in region of 800 nm (non-resonant region) under fs excitation.

Acknowledgements

One of the authors (GJ) is grateful to Dr. Rajan V Anavekar, Former Professor, Department of Physics, Bangalore University, Bangalore, for useful discussions and valuable suggestions. The authors thank Sophisticated Analytical Instrument Facility (SAIF), Indian Institute of Technology, Bombay, India for providing FTIR and HR-TEM experimental facility. Authors would like to thank DST-FIST for providing XRD measurements at Department of Physics, Bangalore University, Bangalore. S. V. Rao thanks DRDO, India for financial support through ACRHEM.

References

[1] A.L. Stepanov, Nonlinear optical properties of metal nanoparticles in silicate glass, in: B. Karmakar, K. Rademann, A.L. Stepanov (Eds.), Glass Nanocomposites, First Ed., Elsevier Publishing, 2016, pp. 165–179.
[2] S. Link, M.A. El-Sayed, J. Phys. Chem. B103 (1999) 8410–8426.
[3] V.E. Ferry, L.A. Sweatlock, H. Domenico Pacifici, A. Atwater, Nano Lett. 8 (2008) 4391–4397.
[4] A.R. Tao, D.P. Ceperley, P. Sinsermsuksakul, A.R. Neureuther, P. Yang, Nano Lett. 8 (2008) 4033–4038.
[5] Ju Seongmin, R. Pramod, Seong Gu Kang Watekar, Jun-Ki Chung, Cheol Jin Kim, Won-Taek Han, J. Non-Cryst. Solids 356 (2010) 2578–2582.
[6] R.A. Ganeev, A.I. Ryasnyansky, A.L. Stepanov, T. Usmanov, Phys. Status Solidi B 241 (2004) R1–R4.
[7] J. Zhong, W. Xiang, H. Zhao, W. Zhao, G. Chen, X. Liang, J. Alloys Compd. 537 (2012) 269–274.
[8] K.J. Ziegler, R. Christopher Doty, K.P. Johnston, B.A. Korgel, J. Am. Chem. Soc. 123 (2001) 7797–7803.
[9] S. Mallick, S. Sharma, M. Banerjee, S.S. Ghosh, A. Chattopadhyay, A. Paul, ACS Appl. Mater. Interfaces 4 (2012) 1313–1323.
[10] A.L. Stepanov, Linear and nonlinear optical properties of silver nanoparticles synthesized in dielectrics by ion implantation and laser annealing, in: David Pozo Perez (Ed.), Silver Nanoparticles, INTECH Publishing, 2010, pp. 93–120.
[11] J.W. Jeon, P.A. Ledin, J.A. Geldmeier, J.F. Ponder Jr., M.A. Mahmoud, M. El-Sayed, J.R. Reynolds, V.V. Tsukruk, Chem. Mater. 28 (2016) 2868–2881.
[12] S. Linic, P. Christopher, D.B. Ingram, Nat. Mater. 10 (2011) 911–921.
[13] X. Li, W.C.H. Choy, L. Huo, F. Xie, W.E.I. Sha, B. Ding, X. Guo, Y. Li, J. Hou, J. You, Y. Yang, Adv. Mater. 24 (2012) 3046–3052.
[14] C. An, S. Peng, Y. Sun, Adv. Mater. 22 (2010) 2570–2574.
[15] X. Huang, I.H. El-Sayed, W. Qian, M.A. El-Sayed, J. Am. Chem. Soc. 128 (2006) 2115–2120.
[16] G.J. Nusz, A.C. Curry, S.M. Marinakos, A. Wax, A. Chilkoti, ACS Nano 3 (2009) 795–806.
[17] J.N. Anker, W.P. Hall, O. Lyandres, N.C. Shah, J. Zhao, R.P. Van Duyne, Nat. Mater. 7 (2008) 442–453.
[18] M.R. Dousti, M.R. Sahar, R.J. Amjad, S.K. Ghoshal, A. Khorramnazari, A. Dordizadeh Basirabad, A. Samavati, Eur. Phys. J. D 66 (2012) 237–242.
[19] J. Qiu, X. Jiang, C. Zhu, H. Inouye, J. Si, K. Hirao, Opt. Lett. 29 (2004) 370–372.
[20] C.L. Haynes, R.P. Van Duyne, J. Phys. Chem. B 105 (2001) 5599–5611.
[21] K.S. Lee, M.A. El-Sayed, J. Phys. Chem. B 109 (2005) 20331–20338.
[22] H. Wang, D.W. Brandl, F. Le, P. Nordlander, N.J. Halas, Nano Lett. 6 (2006) 827–832.
[23] T. König, R. Kodiyath, Z.A. Combs, M.A. Mahmoud, M.A. El-Sayed, V.V. Tsukruk, Part. Part. Syst. Charact. 31 (2014) 274–283.
[24] Cid B. de Araujo, Tamara R. Oliveira, Edilson L. Falcao-Filho, Davinson M. Silva, Luciana R.P. Kassab, J. Lumin. 133 (2013) 180–183.
[25] S. Ju, S. Jeong, Y. Kim, P. Jeon, W.-T. Han, S. Boo, P.R. Watekar, Sensors and Transducers, 18 (2013), pp. 76–83.
[26] S. Ju, P.R. Watekar, S. Jeong, Y. Kim, W.T. Han, J. Nanosci. Nanotechnol. 12 (2012) 629–634.
[27] J.M.P. Almeida, D.S. da Silva, L.R.P. Kassab, S.C. Zilio, C.R. Mendonça, L. De Boni, Opt. Mater. 36 (2014) 829–832.
[28] D. Manzani, J.M.P. Almeida, M. Napoli, L. De Boni, M. Nalin, C.R.M. Afonso, S.J.L. Ribeiro, C.R. Mendonça, Plasmonics 8 (2013) 1667–1674.
[29] R.A. Ganeev, A.I. Ryasnyanski, A.L. Stepanov, T. Usmanov, C. Marques, R.C. da Silva, E. Alves, Opt. Spectrosc. 101 (2006) 615–622.
[30] A.I. Ryasnyansky, B. Palpant, S. Debrus, R.I. Khaibullin, A.L. Stepanov, J. Opt. Soc. Am. B 23 (2006) 1348–1353.
[31] Y. Takeda, O.A. Plaksin, K. Kono, N. Kishimoto, Surf. Coat. Technol. 196 (2005) 30–33.
[32] A. Cetin, R. Kibar, M. Hatipoglu, Y. Karabulut, N. Can, Phys. B Condens. Matter 405 (2010) 2323–2325.
[33] V.T. Adamiv, I.M. Bolesta, V. Ya, R.V. Burak, I.D. Gamernyk, I.I. Karbovnyk, M.G. Kolych, O.O. Kovalchuk, M.V. Kushnir, I. Periv, M. Teslyuk, Phys. B Condens. Matter 449 (2014) 31–35.
[34] B.V. Padlyak, N.A. Sereev, M. Olczeski, V.T. Adamiv, Ya V. Burak, Phys. Chem. Glasses: Eur. J. Glass Sci. Technol., Part B 55 (2014) 25–33.
[35] R.E. Youngman, J.W. Zwanziger, J. Non-Cryst. Solids 168 (1994) 293–297.
[36] R.E. Youngman, S.T. Haubrich, J.W. Zwanziger, M.T. Janicke, B.F. Chemelka, Science 269 (1995) 1416–1419.
[37] M. Sheik-Bahae, A.A. Said, Tai-Huei Wei, D.J. Hagan, E.W. Van Stryland, IEEE J. Quantum Electron. 26 (1990) 760–769.
[38] S.K. Ghoshal, Asmahani Awang, M.R. Sahar, R. Arifin, J. Lumin. 159 (2015) 265–273.
[39] K.T. Arulmozhi, N. Mythili, AIP Adv. 3 (2013) 1–9.
[40] J. Sasai, K. Hirao, J. Appl. Phys. 89 (2001) 4548–4552.
[41] K. Keshavamurthy, B. Eraiah, Bull. Mater. Sci. 38 (2015) 1381–1384.
[42] M. Farouk, A. Samir, F. Metawe, M. Elokr, Non-Cryst. Solids 371–372 (2013) 14–21.
[43] E.A. Davis, N.F. Motto, Philos. Mag. 22 (1970) 903–922.
[44] M. Altaf, M.A. Chaudhry, S.A. Siddiqi, Glas. Phys. Chem. 31 (2005) 597–601.
[45] P. Mulvaney, Langmuir 12 (1996) 788–800.
[46] S. Ju, S. Jeong, Y. Kim, S.-H. Lee, W.-T. Han, J. Nanosci. Nanotechnol. 15 (2016) 1–5.
[47] J. Homola, S.S. Yee, G. Gauglitz, Sensors Actuators B Chem. 5 (1999) 3–15.
[48] S. Ju, S. Jeong, Y. Kim, P. Jeon, W.-T. Han, S. Boo, P.R. Watekar, The Third International Conference on Sensor Device Technologies and Applications, (2012) Proceedings pp 89–94 ISBN: 978-1-61208-208-0.
[49] R.J. Amjad, M.R. Dousti, M.R. Sahar, S.F. Shaukat, S.K. Ghoshal, E.S. Sazali, Fakhra Nawaz, J. Lumin. 154 (2014) 316–321.
[50] A. Pana, Z. Yang, H. Zheng, F. Liu, Y. Zhu, X. Su, Z. Ding, Appl. Surf. Sci. 205 (2003) 323–328.
[51] J.C. Maxwell Garnett, Philos. Trans. R. Soc. London, Ser. A (1906) 205237.
[52] M. Fox, Optical Properties of Solids, Oxford University Press, U S, 2007.
[53] M.R. Dousti, M.R. Sahar, S.K. Ghoshal, R.J. Amjad, A.R. Samavati, J. Mol. Struct. 1035 (2013) 6–12.
[54] B. Eraiah, Bull. Mater. Sci. 29 (2006) 375–378.
[55] R.J. Amjad, M.R. Sahar, M.R. Dousti, S.K. Ghoshal, M.N.A. Jamaludin, Opt. Exp. 21 (2013) 14282–14290.
[56] G. Upender, S. Ramesh, M. Prasad, V.G. Sathe, V.C. Mouli, J. Alloys Compd. 504 (2010) 468–474.
[57] H.A.A. Sidek, S. Rosmawati, Z.A. Talib, M.K. Halimah, W.M. Daud, Am. J. Appl. Sci. 6 (2009) 1489–1494.
[58] G. Kaur, M. Kumar, A. Arora, O.P. Pandey, K. Singh, J. Non-Cryst. Solids 357 (2011) 858–863.
[59] P. Chimalawong, J. Kaewkhao, C. Kedkaew, P. Limsuwan, J. Phys. Chem. Solids 71 (2010) 965–970.
[60] S.G. Motke, S.P. Yawale, S.S. Yawale, Bull. Mater. Sci. 25 (2002) 75–78.
[61] J. Krogh-Moe, J. Non-Cryst. Solids 1 (1969) 269–284.
[62] K. El-Egili, A.H. Oraby, J. Phys. Condens. Matter. 8 (1996) 8959–8970.
[63] A.R. Kulkarni, H.S. Maiti, A. Paul, Bull. Mater. Sci. 6 (1984) 201–221.
[64] B. Karthikeyan, C.S. Suchand Sandeep, J. Cha, H. Takebe, R. Philip, S. Mohan, J. Appl. Phys. 103 (2008) 1–6.
[65] T. Som, B. Karmakar, Antimony oxide glasses and their nanocomposites for optical, photonic and nanophotonic applications, in: M. Razeghi (Ed.), Antimony: Characteristics, Compounds and Applications, Nova Publishers, ebook, 2012, pp. 1–40.
[66] T. Som, B. Karmakar, J. Opt. Soc. Am. B 26 (2009) B21–B27.
[67] D.R. Lide, CRC Handbook of Chemistry and Physics, 75th ed., CRC Press, 1975, pp. 8–34.
[68] O. Smithies, M. Lawrence, A. Testen, L.P. Horne, J. Wilder, M. Altenburg, B. Bleasdale, N. Maeda, T. Koklic, Langmuir 30 (2014) 13394–13404.
[69] G. Lusvardi, G. Malavasi, V. Aina, L. Bertinetti, G. Cerrato, G. Magnacca, C. Morterra, L. Menabue, Langmuir 26 (2010) 10303–10314.
[70] S. Qu, Y. Gao, X. Jiang, H. Zeng, Y. Song, J. Qiu, C. Zhu, K. Hirao, Opt. Commun. 224 (2003) 321–327.
[71] R. Sai Santosh, S. Kumar, L. Venugopal Rao, D. Giribabu, Narayana Rao, Chem. Phys. Lett. 447 (2007) 274–278.
[72] R.L. Sutherland, Handbook of Nonlinear Optics, 2nd ed., Marcel Dekker, New York, 2003 (Revised and Expanded).
[73] X. Zhu, N. Qi Li, Z. Ming, Meng, Appl. Phys. Lett. 71 (1997) 867–869.
[74] R. Rajaramakrishna, S. Karuthedath, R.V. Anavekar, H. Jain, J. Non-Cryst. Solids 358 (2012) 1667–1672.
[75] B. Shanmugavelu, V.V. Ravi Kanth Kumar, R. Kuladeep, D. Narayana Rao, J. Appl. Phys. 114 (2013) 1–6.
[76] N. Venkatram, R. Sai Santosh Kumar, D. Narayana Rao, S.K. Medda, S. De, G. De, J. Nanosci. Nanotechnol. 6 (2006) 1990–1994.
[77] U. Gurudas, E. Brooks, D.M. Bubb, S. Heiroth, T. Lippert, A. Wokaun, J. Appl. Phys. 104 (2008) 1–8.
[78] R. Philip, P. Chantharasupawong, H. Qian, R. Jin, J. Thomas, Nano Lett. 12 (2012) 4661–4667.